Int. J. Electrochem. Sci., 15 **(2020)** 8732 – 8742, doi: 10.20964/2020.09.61

International Journal of
ELECTROCHEMICAL
SCIENCE
www.electrochemsci.org

Enhanced Electrochemical Properties of Titanium Doped Lithium Manganese Oxide with Nanorod-like Morphology

Jing Xue[*], *Hu Zhang, Tuoying Yang, Xiuxing Zhang*

Shaanxi X-ray Detection and Application Research and Development Center, School of Physics and Electrical Engineering, Weinan Normal University, Weinan 714099, China
[*]E-mail: xuejingwnu@126.com

Received: 10 May 2020 / *Accepted:* 13 July 2020 / *Published:* 10 August 2020

The Ti-doped $LiMn_2O_4$ ($LiMn_{1.97}Ti_{0.03}O_4$) nanorods are prepared by self-sacrificial template method with titanium dioxide (TiO_2) nanoparticles and manganese hydroxide (γ-MnOOH) nanorods as doping agent and manganese precursor, respectively. The obtained $LiMn_{1.97}Ti_{0.03}O_4$ nanorods possess obvious nanorod structure and no other impurity peaks can be observed in the XRD pattern of the titanium doped sample, which suggests the successful inheritance of nanorod structure of γ-MnOOH in the $LiMn_{1.97}Ti_{0.03}O_4$ sample with high purity. According to the electrochemical results, the $LiMn_{1.97}Ti_{0.03}O_4$ nanorods present excellent cycling performance. When tested at 0.5 C, the $LiMn_{1.97}Ti_{0.03}O_4$ nanorods show an initial discharge capacity of 125.1 mAh g^{-1} with high capacity retention of 93.8% after 100 cycles. Moreover, the $LiMn_{1.97}Ti_{0.03}O_4$ nanorods show better rate performance and cycling stability under high temperature. This work indicates that the co-modification of Ti-doping and nanorod morphology has synergistic effect, which can effectively help enhance the electrochemical properties of $LiMn_2O_4$.

Keywords: Lithium manganese oxide; Ti-doping; Nanorod-like morphology; Synergistic effect; Cycling stability

1. INTRODUCTION

Manganese-based cathode materials have been widely recognized as the promising cathode materials due to the abundant manganese resources and high cost effectiveness [1-5]. At present, scientific researchers have developed various manganese-based cathode materials such as orthorhombic $LiMnO_2$, spinel $LiMn_2O_4$, Li-rich layered Li_2MnO_3, and its composites [6-10]. Among them, spinel $LiMn_2O_4$ has been successfully applied as commercial cathode material for lithium-ion battery. However, it is worth noting that the poor cycling performance of this material can not meet the

requirement for long battery life. In particular, $LiMn_2O_4$ suffers a severe capacity loss at high temperatures [11-14].

In order to improve the cycling stability, scientific researchers have developed various modification strategies, such as body-doping, surface modification, and morphology control, etc [15-17]. Among these strategies, the body-doping has attracted a great deal of attention for material modification. With regard to spinel $LiMn_2O_4$, trivalent manganese ions (Mn^{3+}) can lead to the Jahn-Teller distortion, which has some serious implications for the structural stability of $LiMn_2O_4$ during the charge-discharge process [9, 18]. To inhibit the Jahn-Teller distortion, plenty of heterogeneous ions (Cu^{2+}, Zn^{2+}, Al^{3+}, Er^{3+}, Si^{4+}, Ti^{4+}, etc.) have been introduced in the crystal structure of $LiMn_2O_4$ to partly replace the Mn^{3+} ions [9, 14, 15, 19-21]. As a result, the structural stability of $LiMn_2O_4$ has been enhanced to a certain extent due to the inhibition of Jahn-Teller distortion of Mn^{3+} ions. However, note that the introduction of low-value heterogeneous ions can lead to some negative influence upon the reversible capacity [15, 22]. According to the existing literatures [9, 20, 23], the body-doping with high-value heterogeneous ions (Si^{4+}, Ti^{4+}) can reduce this negative impact on the reversible capacity to a certain extent since the high-value heterogeneous ions only replace the tetravalent manganese ions. Moreover, the nanorod morphology can effectively improve the electrochemical performance of $LiMn_2O_4$ because of the facilitation of one-dimensional transport pathway on the electron transport [17, 24, 25]. Therefore, it is necessary to consider the comprehensive utilization of high-value heterogeneous ions-doping and nanorod morphology to improve the electrochemical performance of $LiMn_2O_4$.

In this work, the $LiMn_{1.97}Ti_{0.03}O_4$ nanorods were prepared by self-sacrificial template method with titanium dioxide (TiO_2) nanoparticles and manganese hydroxide (γ-MnOOH) nanorods as doping agent and manganese precursor, respectively. The phase structures, surface morphologies and electrochemical properties of the obtained samples are studied. This work provides a valuable reference for the application of $LiMn_2O_4$.

2. EXPERIMENTAL

The $LiMn_{1.97}Ti_{0.03}O_4$ nanorods were prepared through a self-sacrificial template synthetic route with titanium dioxide (TiO_2) nanoparticles and manganese hydroxide (γ-MnOOH) nanorods as titanium-doping source and self-sacrificial manganese precursor, respectively. Briefly, the γ-MnOOH nanorods were firstly synthesized by hypothermal method based on the existing literature [25]. In a typical process, 4.5 g potassium permanganate ($KMnO_4$) was dissolved in 100 ml deionized water, and 7.5 ml anhydrous alcohol (CH_3CH_2OH) was added to the above solution. After magnetic stirring for 30 min, the obtained solution was transferred into the hydrothermal synthesis reactor (150 ml), which was heated in an oven at 150 °C for 20 h. The γ-MnOOH nanorods were obtained after purification and drying treatment. To prepare the $LiMn_{1.97}Ti_{0.03}O_4$ nanorods, a certain amount of γ-MnOOH nanorods, TiO_2 nanoparticles, $LiOH{\cdot}H_2O$ were weighed according to the corresponding stoichiometric ratio (Li excess: 5%). After mixing them by the aid of absolute ethanol, the obtained mixture was further calcinated at 750 °C for 10 h in air, and the up-and-down temperature rate is 5 ℃/ min. Furthermore, the $LiMn_2O_4$

nanorods were prepared through the same self-sacrificial template synthetic route. The undoped $LiMn_2O_4$ particles were prepared by using electrolytic MnO_2 manganese precursor, and the sintering conditions is same with that of $LiMn_{1.97}Ti_{0.03}O_4$ nanorods and $LiMn_2O_4$ nanorods. **Table 1** lists the comparison of these three samples.

The phase structure and surface morphology have much to do with the electrochemical performance of $LiMn_2O_4$. The corresponding results were obtained by the aid of X-ray diffraction (XRD) and scanning electron microscope (SEM) techniques. The influence of titanium doping and nanorod morphology on the electrochemical performance of $LiMn_2O_4$ were investigated in detail.

Table 1. Comparison of $LiMn_{1.97}Ti_{0.03}O_4$ nanorods, $LiMn_2O_4$ nanorods, and $LiMn_2O_4$ particles.

Sample	Synthesis method	Manganese source	Lithium source	Dopant	Reaction condition
$LiMn_{1.97}Ti_{0.03}O_4$ nanorods	Solid-state	γ-MnOOH nanorods	$LiOH·H_2O$	TiO_2 nanoparticles	750 °C, 10 h
$LiMn_2O_4$ nanorods	Solid-state	γ-MnOOH nanorods	$LiOH·H_2O$	None	750 °C, 10 h
$LiMn_2O_4$ particles	Solid-state	Electrolytic MnO_2	$LiOH·H_2O$	None	750 °C, 10 h

3. RESULTS AND DISCUSSION

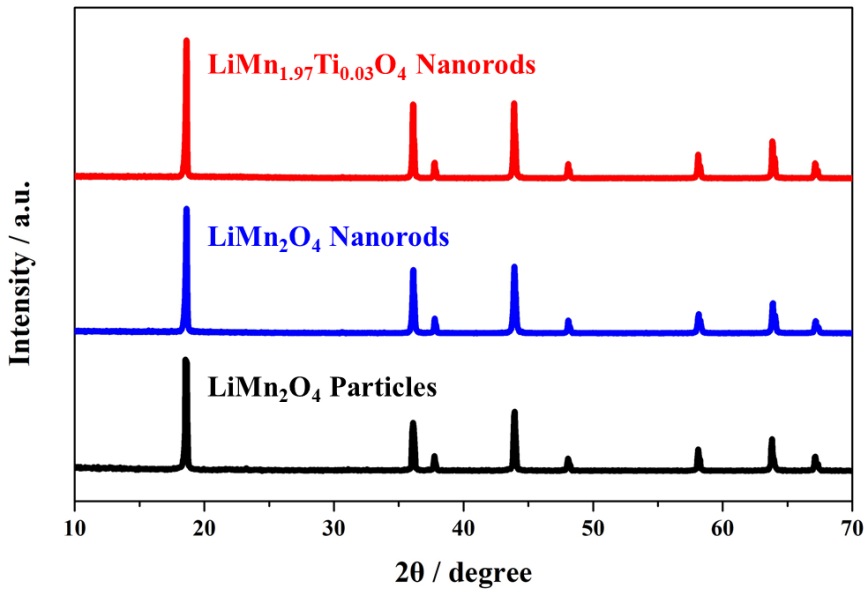

Figure 1. XRD patterns of the $LiMn_2O_4$ particles, $LiMn_2O_4$ nanorods and $LiMn_{1.97}Ti_{0.03}O_4$ nanorods.

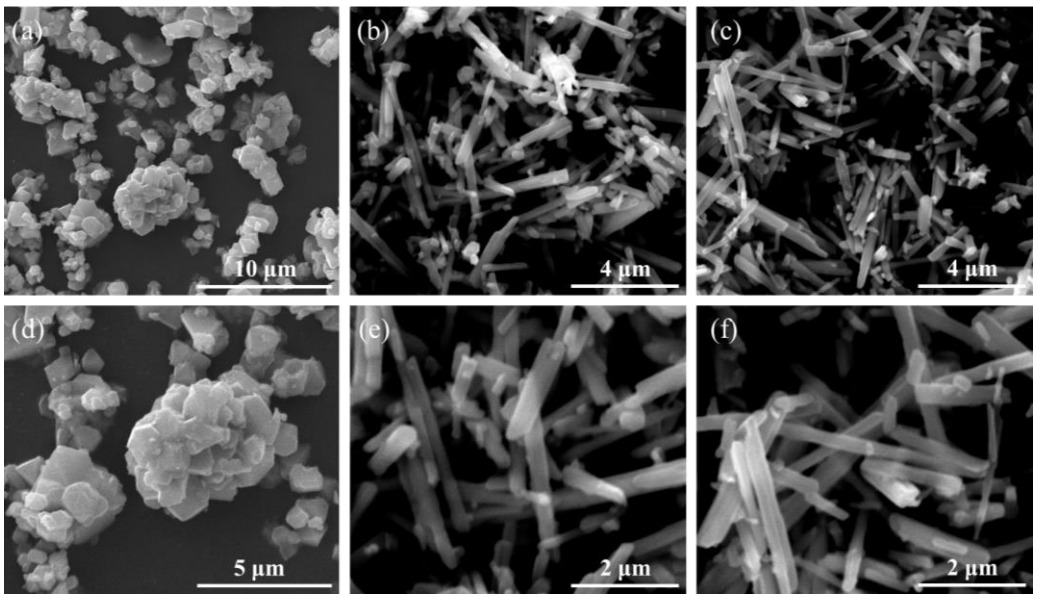

Figure 2. SEM images of the $LiMn_2O_4$ particles (a, b), $LiMn_2O_4$ nanorods (c, d) and $LiMn_{1.97}Ti_{0.03}O_4$ nanorods.

Figure 1 shows the XRD patterns of the $LiMn_2O_4$ particles, $LiMn_2O_4$ nanorods and $LiMn_{1.97}Ti_{0.03}O_4$ nanorods. It can be clearly observed that the undoped $LiMn_2O_4$ particles and $LiMn_2O_4$ nanorods present obvious diffraction peaks, which can be indexed to $LiMn_2O_4$ (JCPDS No. 35-0782) [9, 26]. No other impurity peaks can be observed in the XRD patterns of these two $LiMn_2O_4$ samples, suggesting the successful transformation of electrolytic MnO_2 and γ-MnOOH nanorods into the spinel $LiMn_2O_4$ samples with high purity [17, 25]. After introducing a certain amount of Ti^{4+} ions, the $LiMn_{1.97}Ti_{0.03}O_4$ nanorods show obvious diffraction peaks, which suggests that Ti-doping has no important impact on the crystal structure of $LiMn_2O_4$.

Figure 2 shows the SEM images of the $LiMn_2O_4$ particles, $LiMn_2O_4$ nanorods and $LiMn_{1.97}Ti_{0.03}O_4$ nanorods. As shown in Figure 2a and c, the $LiMn_2O_4$ particles show irregular particle size distribution. There are some agglomerated particles, which consists of the irregular $LiMn_2O_4$ particles. These features can lead to serious negative impact on the cycling performance of $LiMn_2O_4$ [14]. By contrast, the $LiMn_2O_4$ nanorods and $LiMn_{1.97}Ti_{0.03}O_4$ nanorods possess evident nanorod-like morphology, which suggests that the nanorod structure of γ-MnOOH is well maintained in the $LiMn_2O_4$-based samples [17]. According to the existing literatures [25], both the $LiMn_2O_4$ nanorods and $LiMn_{1.97}Ti_{0.03}O_4$ nanorods may show excellent electrochemical performance due to the facilitation of one-dimensional transport pathway on the electron transport rate.

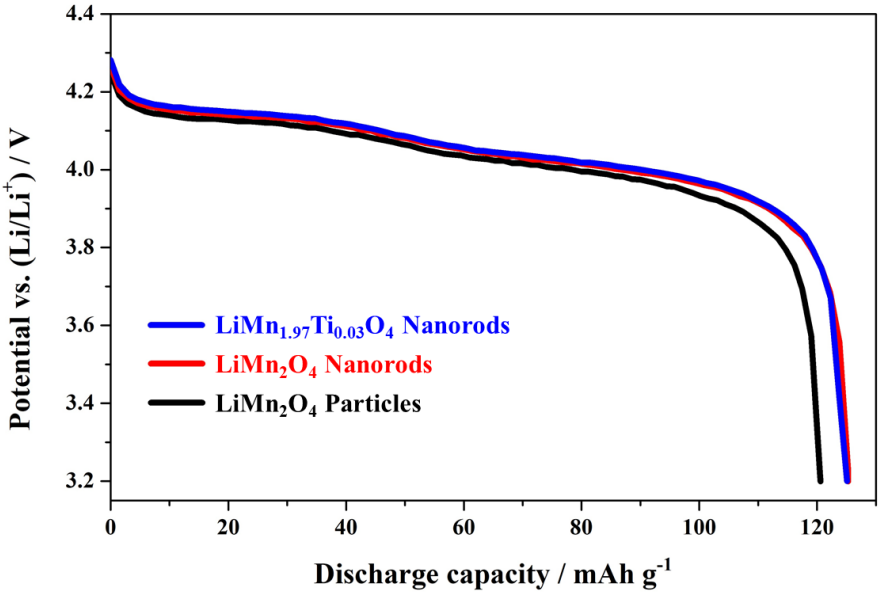

Figure 3. Initial charge-discharge curves of the $LiMn_2O_4$ particles, $LiMn_2O_4$ nanorods and $LiMn_{1.97}Ti_{0.03}O_4$ nanorods cycled at 0.5 C.

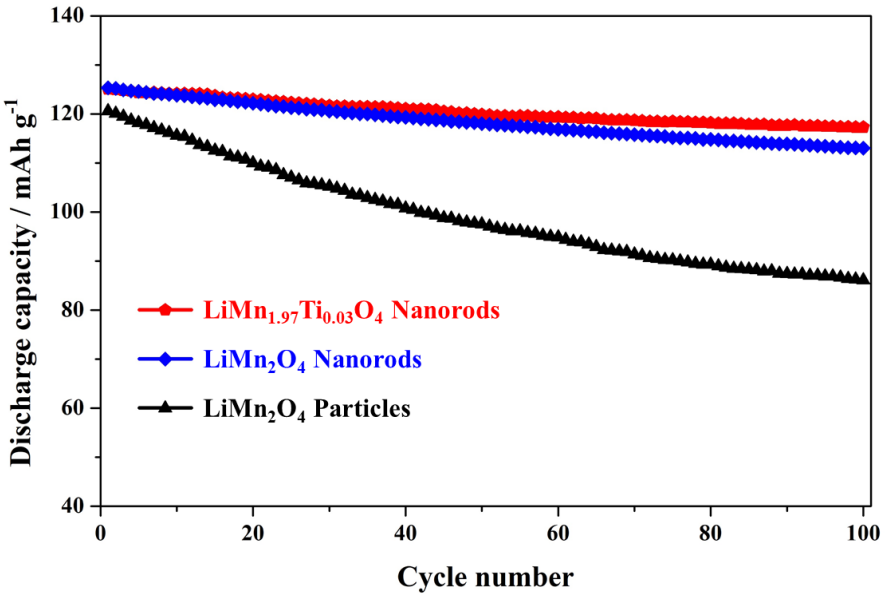

Figure 4. Cycling stability of the $LiMn_2O_4$ particles, $LiMn_2O_4$ nanorods and $LiMn_{1.97}Ti_{0.03}O_4$ nanorods cycled at 0.5 C.

According to the existing literatures [17, 20], both the Ti-doping and nanorod-like morphology often result in a positive impact to the electrochemical performance of $LiMn_2O_4$ cathode material. To study the influence of the co-modification of Ti-doping and nanorod-like morphology on the cycling stability, the $LiMn_2O_4$ particles, $LiMn_2O_4$ nanorods and $LiMn_{1.97}Ti_{0.03}O_4$ nanorods were cycled at 0.5 C. Figure 3 shows the corresponding initial charge-discharge curves of these three samples. As shown here,

the discharge curves of the undoped $LiMn_2O_4$ samples show two voltage plateaus, which have much to do with the two-phase equilibrium of λ-MnO_2/$Li_{0.5}Mn_2O_4$ and single-phase equilibrium of $Li_{0.5}Mn_2O_4$/$LiMn_2O_4$, respectively [27, 28]. For the $LiMn_{1.97}Ti_{0.03}O_4$ nanorods, the voltage plateaus of the initial charge-discharge curve agree with that of the undoped samples, suggesting that the introduction of a certain amount of Ti^{4+} ions has no great effect on the transformation of phase structure during the charge-discharge process [14, 20].

The cycling stability constrains the practical application of $LiMn_2O_4$ cathode materials to a large extent. Figure 4 shows the cycling performance of the $LiMn_2O_4$ particles, $LiMn_2O_4$ nanorods and $LiMn_{1.97}Ti_{0.03}O_4$ nanorods. As shown here, the undoped $LiMn_2O_4$ particles exhibit a less-than-satisfactory initial discharge capacity of 120.6 mAh g^{-1}. After 100 cycles, the discharge capacity of this sample only reaches up to 86.1 mAh g^{-1} with rather low capacity retention rate of 71.4%. This result has much to do with the irregular particle size distribution of $LiMn_2O_4$ particles, especially some agglomerated particles [29]. By contrast, the $LiMn_2O_4$ nanorods can show slightly higher reversible capacity and better cycling performance than that of the $LiMn_2O_4$ particles due to the facilitation of one-dimensional transport pathway on the electron transport rate [17, 25]. The initial discharge capacity of the $LiMn_2O_4$ nanorods can reach up to 125.3 mAh g^{-1} with capacity retention of 90.2% after 100 cycles. For the $LiMn_{1.97}Ti_{0.03}O_4$ nanorods, the initial discharge capacity has no significant reduction because the introduction of a certain amount of Ti^{4+} ions avoids the reduction of trivalent manganese ions, which have much to do with the reversible capacity of $LiMn_2O_4$ [20, 23]. Moreover, the cycling stability of the $LiMn_{1.97}Ti_{0.03}O_4$ nanorods is further enhanced with quite high capacity retention rate of 93.8% compared to the $LiMn_2O_4$ nanorods. Table 2 compares the cycling performance of the $LiMn_{1.97}Ti_{0.03}O_4$ nanorods and other reported $LiMn_2O_4$-based cathode materials [20, 25]. It can be observed that the combination of Ti-doping and nanorod-like morphology has important meaning for improving the cycling performance of $LiMn_2O_4$ cathode materials. Compared with some reported $LiMn_2O_4$-based cathode materials, the $LiMn_{1.97}Ti_{0.03}O_4$ nanorods can show excellent cycling performance with high capacity retention. Such high performance is mainly contributed by the synergistic effect of Ti-doping and nanorod-like morphology. The introduction of a certain amount of Ti^{4+} ions can effectively improve the structural stability [20], and the one-dimensional transport pathway of nanorod-like morphology can promote the charge transfer [17]. Based on the synergistic interaction of Ti-doping and nanorod-like morphology, the $LiMn_{1.97}Ti_{0.03}O_4$ nanorods show excellent cycling stability with high capacity retention.

Table 2. Comparison of $LiMn_{1.97}Ti_{0.03}O_4$ nanorods and other reported $LiMn_2O_4$-based cathode materials.

Sample	Cycling condition	Initial capacity (mAh g-1)	Capacity retention (%)	Reference
$LiMn_{1.97}Ti_{0.03}O_4$ nanorods	0.5 C, 100 cycles	125.1	93.8	This work
$LiMn_2O_4$ nanorods	1.0 C, 100 cycles	123.5	89.2	[25]
Ti-doped $LiMn_2O_4$ particles	0.5 C, 70 cycles	135.7	95	[20]

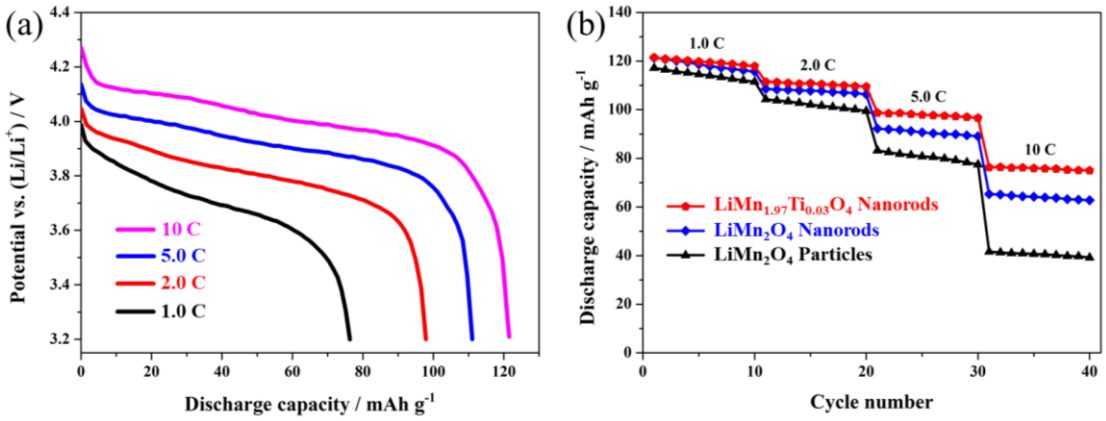

Figure 5. (a) Representative discharge curves of the $LiMn_{1.97}Ti_{0.03}O_4$ nanorods and (b) Rate capability of the $LiMn_2O_4$ particles, $LiMn_2O_4$ nanorods and $LiMn_{1.97}Ti_{0.03}O_4$ nanorods.

In order to determine the impact of the co-modification to Ti-doping and nanorod-like morphology on rate capability, the $LiMn_2O_4$ particles, $LiMn_2O_4$ nanorods and $LiMn_{1.97}Ti_{0.03}O_4$ nanorods were cycled at different rates. Figure 5a shows the representative discharge curves of the $LiMn_{1.97}Ti_{0.03}O_4$ nanorods, which are selected as a sample representative. As shown here, the cycling rate show an important impact on the voltage platform and reversible capacity. The increased cycling rate can obscure the boundary of two voltage plateaus and decrease the discharge capacity, which have much to do with the increased polarization [26]. Figure 5b shows the cycling stability of the $LiMn_2O_4$ particles, $LiMn_2O_4$ nanorods and $LiMn_{1.97}Ti_{0.03}O_4$ nanorods cycled at different rates. As shown here, the undoped $LiMn_2O_4$ particles present an unsatisfactory rate capability. When cycled at 1.0 C, this undoped sample can show an initial discharge capacity of 117.2 mAh g^{-1}. However, as the cycling rate increases to 5.0 C, the discharge capacity of this sample rapidly decreases to 83.2 mAh g^{-1} with rather low capacity retention rate of 71.0%. By contrast, the $LiMn_2O_4$ nanorods can show better rate performance. When cycled at 5.0 C, the discharge capacity of the $LiMn_2O_4$ nanorods can reach up to 92.2 mAh g^{-1} with good capacity retention rate of 76.0%. For the $LiMn_{1.97}Ti_{0.03}O_4$ nanorods, the initial discharge capacity has no significant difference, but the excellent rate capability can be observed with the increasing of the cycling rate. When cycled at 5.0 C and 10 C, the discharge capacity of the $LiMn_{1.97}Ti_{0.03}O_4$ nanorods can reach up to 98.7 mAh g^{-1} and 76.3 mAh g^{-1}. Such excellent rate performance is mainly contributed by the improvement of Ti-doping on the structural stability and promotional effect of nanorod-like morphology on the charge transfer [17, 20]. The synergistic interaction of Ti-doping and nanorod-like morphology significantly enhances the rate capability of $LiMn_2O_4$ cathode material.

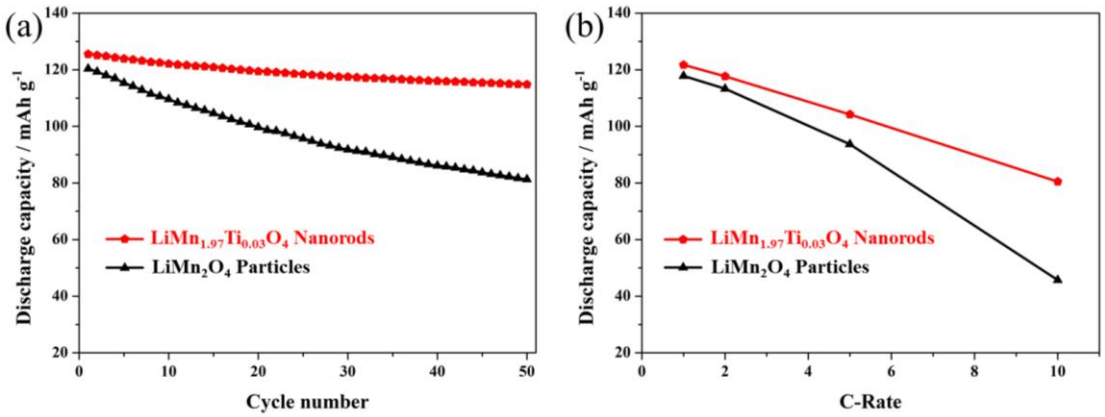

Figure 6. (a) Cycling stability and (b) rate capability of the $LiMn_2O_4$ particles and $LiMn_{1.97}Ti_{0.03}O_4$ nanorods under high temperature (55 °C).

Figure 6a shows the cycling stability of the $LiMn_2O_4$ particles and $LiMn_{1.97}Ti_{0.03}O_4$ nanorods cycled at 55 °C. As shown here, the undoped $LiMn_2O_4$ particles present an initial discharge capacity of 120.4 mAh g^{-1}, which is approximate to that of this sample at room temperature (Figure 4). However, the high temperature has great impact on the cycling performance of the undoped $LiMn_2O_4$ particles. After 100 cycles, the discharge capacity of this sample only reaches up to 81.3 mAh g^{-1} with rather low capacity retention rate of 67.5%. This result has much to do with the irregular particle size distribution of $LiMn_2O_4$ particles, especially some agglomerated particles [30]. By contrast, the $LiMn_{1.97}Ti_{0.03}O_4$ nanorods can show much higher reversible capacity and better cycling performance than that of the undoped $LiMn_2O_4$ particles due to synergistic interaction of Ti-doping and nanorod-like morphology. The introduction of a certain amount of Ti^{4+} ions can effectively enhance the structural stability, and the one-dimensional transport pathway of nanorod-like morphology can promote the charge transfer. The initial discharge capacity of the $LiMn_2O_4$ nanorods can reach up to 125.5 mAh g^{-1} with capacity retention rate of 91.5% after 100 cycles, which suggests the positive effect of the co-modification of Ti-doping and nanorod-like morphology on the high-temperature performance. Figure 6b shows the rate perforamance of the $LiMn_2O_4$ particles, $LiMn_2O_4$ nanorods and $LiMn_{1.97}Ti_{0.03}O_4$ nanorods cycled. As shown here, the undoped $LiMn_2O_4$ particles present an unsatisfactory rate capability. By contrast, the $LiMn_{1.97}Ti_{0.03}O_4$ nanorods can show better rate performance. When cycled at 5.0 C and 10 C, the discharge capacity of the $LiMn_{1.97}Ti_{0.03}O_4$ nanorods can reach up to 104.2 mAh g^{-1} and 80.5 mAh g^{-1} with good capacity retention rate of 85.6% and 66.1%. The above analysis indicates that the co-modification of Ti-doping and nanorod-like morphology can significantly optimize the electrochemical performance of $LiMn_2O_4$ cathode material under high temperature.

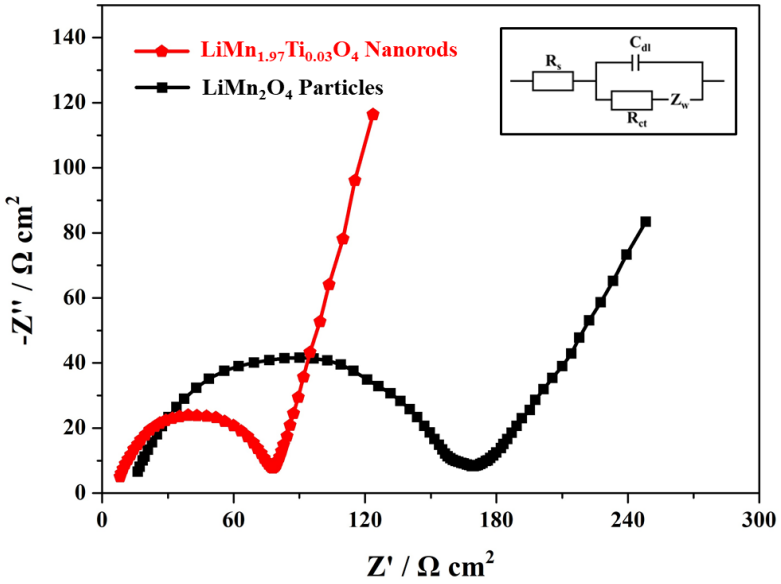

Figure 7. Nyquist plots of the $LiMn_2O_4$ and $LiMn_{1.97}Ti_{0.03}O_4$ nanorods (the insert is the equivalent circuit model of EIS).

Figure 7 shows the EIS results of the $LiMn_2O_4$ particles and $LiMn_{1.97}Ti_{0.03}O_4$ nanorods. According to the equivalent circuit model (The insert in Figure 7), the corresponding fitting values can be obtained to confirm the effect of the co-modification of Ti-doping and nanorod-like morphology on the dynamic process. It has been reported that the charge transfer resistance (R_2) has strong connections with the electrochemical performance of $LiMn_2O_4$ cathode material [12, 31-33]. Thus, the analysis result from the R_2 value can effectively reflect the influence of the co-modification of Ti-doping and nanorod-like morphology on the dynamic process. It can be seen from Figure 7a that the $LiMn_2O_4$ particles present high R_2 values, which agrees with the electrochemical performance of this sample shown in Figure 4 and Figure 5b. By contrast, the $LiMn_{1.97}Ti_{0.03}O_4$ nanorods show much lower R_2 value, which has much to do with the co-modification of Ti-doping and nanorod-like morphology.

4. CONCLUSIONS

In this work, the co-modification of Ti-doping and nanorod-like morphology was applied to improve the electrochemical performance of $LiMn_2O_4$ cathode material. The $LiMn_{1.97}Ti_{0.03}O_4$ nanorods were prepared by self-sacrificial template method. Compared with the $LiMn_2O_4$ particles, the $LiMn_{1.97}Ti_{0.03}O_4$ nanorods possess more stable crystal structure and more efficient charge transfer rate. When tested at 0.5 C, the capacity retention of the $LiMn_{1.97}Ti_{0.03}O_4$ nanorods can reach up to 93.8% after 100 cycles. Moreover, the $LiMn_{1.97}Ti_{0.03}O_4$ nanorods show better rate performance and high-temperature cycling performance. This work provides a valuable idea to promote the development of high-performance $LiMn_2O_4$ cathode material.

ACKNOWLEDGMENTS
This work was financially supported by Natural science talent program of Weinan Normal University (No. 18ZRRC01), and Shaanxi Key Research and Development Project (No. 2019TSLGY07-05).

References

1. H. Zhao, J. Wang, G. Wang, S. Liu, M. Tan, X. Liu, S. Komarneni, *Ceram. Int*., 43 (2017) 10585.
2. H. Zhao, S. Liu, X. Liu, M. Tan, Z. Wang, Y. Cai, S. Komarneni, *Ceram. Int*., 42 (2016) 9319.
3. X. Yu, J. Deng, X. Yang, J. Li, Z.-H. Huang, B. Li, F. Kang, *Nano Energy*, 67 (2020) 104256.
4. H. Liu, R. Tian, Y. Jiang, X. Tan, J. Chen, L. Zhang, Y. Guo, H. Wang, L. Sun, W. Chu, *Electrochim. Acta*, 180 (2015) 138.
5. Y. Fu, H. Jiang, Y. Hu, Y. Dai, L. Zhang, C. Li, *Ind. Eng. Chem. Res*., 54 (2015) 3800.
6. M.J. Lee, S. Lee, P. Oh, Y. Kim, J. Cho, , *Nano Lett.*, 14 (2014) 993.
7. H. Zhao, B. Chen, C. Cheng, W. Xiong, Z. Wang, Z. Zhang, L. Wang, X. Liu, *Ceram. Int*., 41 (2015) 15266.
8. N. Guerrini, L. Jin, J.G. Lozano, K. Luo, A. Sobkowiak, K. Tsuruta, F. Massel, L.-C. Duda, M.R. Roberts, P.G. Bruce, *Chem. Mater*., 32 (2020) 3733.
9. H. Zhao, S. Liu, Z. Wang, Y. Cai, M. Tan, X. Liu, *Ceram. Int*., 42 (2016) 13442.
10. H. Xia, Z. Luo, J. Xie, *Prog. Nat. Sci.-Mater*., 22 (2012) 572.
11. M. Michalska, D.A. Ziółkowska, J.B. Jasiński, P.H. Lee, P. Ławniczak, B. Andrzejewski, A. Ostrowski, W. Bednarski, S.H. Wu, J.Y. Lin, *Electrochim. Acta*, 276 (2018) 37.
12. J. Liu, G. Li, Y. Yu, H. Bai, M. Shao, J. Guo, C. Su, X. Liu, W. Bai, *J Alloy. Compd*., 728 (2017) 1315-1328.
13. H. Zhao, Y. Nie, Y. Li, T. Wu, E. Zhao, J. Song, S. Komarneni, *Ceram. Int*., 45 (2019) 17183.
14. H. Zhao, X. Gao, Y. Li, Q. Ran, C. Fu, Y. Feng, J. Liu, X. Liu, J. Su, *Ceram. Int*., 45 (2019) 17591.
15. J.L. Wang, Z.H. Li, J. Yang, J.J. Tang, J.J. Yu, W.B. Nie, G.T. Lei, Q.Z. Xiao, *Electrochim. Acta*, 75 (2012) 115.
16. S. Lee, Y. Cho, H.K. Song, K.T. Lee, J. Cho, *Angew Chem. Int. Ed. Engl.*, 51 (2012) 8748.
17. D. Zhan, Q. Zhang, X. Hu, G. Zhu, T. Peng, *Solid State Ionics*, 239 (2013) 8.
18. D. Capsoni, M. Bini, G. Chiodelli, V. Massarotti, P. Mustarelli, L. Linati, M.C. Mozzati, C.B. Azzoni, *Solid State Commun*., 126 (2003) 169.
19. H. Zhao, F. Li, X. Bai, T. Wu, Z. Wang, Y. Li, J. Su, *Materials*, 11 (2018) 1302.
20. L. Xiong, Y. Xu, C. Zhang, Z. Zhang, J. Li, J. *Solid State Electr*., 15 (2011) 1263.
21. H. Zhao, X. Bai, J. Wang, D. Li, B. Li, Y. Wang, L. Dong, B. Liu, S. Komarneni, *Materials*, 11 (2018) 1558.
22. H. Zhao, Y. Nie, D. Que, Y. Hu, Y. Li, *Materials*, 12 (2019) 2807.
23. A. Iturrondobeitia, A. Goñi, L. Lezama, C. Kim, M. Doeff, J. Cabana, T. Rojo, *J. Mater. Chem*. A, 1 (2013) 10857.
24. W. Tang, Y. Hou, F. Wang, L. Liu, Y. Wu, K. Zhu, *Nano Lett*., 13 (2013) 2036.
25. H. Zhao, F. Li, X. Liu, W. Xiong, B. Chen, H. Shao, D. Que, Z. Zhang, Y. Wu, , *Electrochim. Acta*, 166 (2015) 124.
26. H. Zhao, S. Liu, Y. Cai, Z. Wang, M. Tan, X. Liu, *J. Alloy. Compd*., 671 (2016) 304.
27. S. Wang, M. Xiang, Y. Lu, J. Guo, C. Su, H. Bai, X. Liu, *J. Mater. Sci-Mater. El*., 31 (2020) 6036.
28. Y. Yu, M. Xiang, J. Guo, C. Su, X. Liu, H. Bai, W. Bai, K. Duan, *J. Colloid. Interf. Sci*., 555 (2019) 64.
29. X. Liang, S. Zeng, Y. Liu, L. Shi, T. Liu, *Mater. Sci. Tech.-Lond*, 31 (2015) 443.
30. H. Zhao, S. Liu, Z. Wang, Y. Cai, M. Tan, X. Liu, *Electrochim. Acta*, 199 (2016) 18.
31. J. Liu, G. Li, H. Bai, M. Shao, C. Su, J. Guo, X. Liu, W. Bai, *Solid State Ionics*, 307 (2017) 79.

32. A. Iqbal, Y. Iqbal, A.M. Khan, S. Ahmed, *Ionics*, 23 (2017) 1995.
33. R. Thirunakaran, G.H. Lew, W.-S. Yoon, *Powder Technol*., 301 (2016) 197